MALAYSIAN JOURNAL OF MICROSCOPY

Journal homepage: https://malaysianjournalofmicroscopy.org

RESEARCH ARTICLE

DISTRIBUTION OF IRON SAND BASED ON SUSCEPTIBILITY VALUES IN ULAKAN TAPAKIS, PADANG PARIAMAN, WEST SUMATRA

Adree Octova[1,2], Mohd Hazizan Mohd Hashim[1,*], Rika Ampuh Hadiguna[3], Muhammad Irman Khalif Ahmad Aminuddin[1], Yoszi Mingsi Anaperta[2], Lulu Dwi Oktari[2]

[1]Strategic Mineral Niche, School of Material and Mineral Resources Engineering, Universiti Sains Malaysia, 14300 Nibong Tebal, Penang, Malaysia.

[2]Department of Mining Engineering, Faculty of Engineering, Universitas Negeri Padang, Jl. Prof. Hamka, Padang 25131, Indonesia.

[3]Engineer Professional Education, Graduate School, Universitas Andalas, Limau Manis, Padang 25175, Indonesia.

Abstract. This study investigates the distribution of iron sand deposits in the Ulakan Tapakis coastal area, Padang Pariaman, West Sumatra, based on magnetic susceptibility values. The region is known for its abundant but underutilized iron sand resources. Previous studies have not sufficiently examined the correlation between magnetic susceptibility and mineralogical composition, which is crucial for optimizing extraction. This research addresses that gap by integrating field sampling, laboratory analysis, and microscopy examination. Twenty borehole samples were collected using a hand auger method arranged in four parallel and five perpendicular transects along the coastline. The magnetic mineral content was determined by magnetic separation, and magnetic susceptibility was measured using the Bartington MS2B sensor at both low and high field settings. Results revealed significant spatial variability, with the highest magnetic mineral content (28.63%) and susceptibility values (5574.8×10^{-8} m^3/kg) observed at point 1D. Microscopy analysis of this sample confirmed the presence of iron (Fe) and zirconium (Zr) minerals, with Fe comprising 79.98% of the material. These findings indicate a heterogeneous distribution of magnetic minerals influenced by lithological and depositional conditions. The integration of susceptibility measurements and mineralogical data provides a practical framework for identifying high-potential extraction zones. The outcomes support the development of targeted mineral exploration strategies and sustainable resource management practices in similar coastal environments. Future research should aim to incorporate advanced imaging techniques for better characterization and explore broader industrial applications of iron sand.

Keywords: Iron sand, magnetic susceptibility, mineral composition, microscopy analysis, ulakan tapakis.

Article Info

Received 25 August 2024
Accepted 23 May 2025
Published 2 June 2025

***Corresponding author: mohd_hazizan@usm.my**

ISSN: 1823-7010, eISSN: 2600-7444

1. INTRODUCTION

The west coast of West Sumatra, including the Ulakan Tapakis region in Padang Pariaman, is endowed with extensive deposits of iron sand. Despite the abundance of this mineral resource, it remains significantly underutilized. Local communities have expressed concerns regarding the potential environmental impact of mining activities, particularly coastal erosion, which has led to the resource being largely untapped. However, with proper management, the iron sand deposits could play a crucial role in regional industrial development, providing raw materials for various industries and boosting the local economy.

Previous studies on the Ulakan Tapakis area have primarily used resistivity methods to map iron sand distribution, revealing deposits at depths of 0.7 to 3 meters with resistivity values between 52 Ωm and 289 Ωm [1]. However, these studies did not examine how magnetic susceptibility correlates with mineralogical composition, creating a gap in understanding the distribution of iron-bearing minerals in this region. A comprehensive analysis that incorporates magnetic susceptibility data is essential to optimize extraction strategies and minimize environmental impacts.

The main research problem addressed in this study is the lack of a comprehensive model depicting the distribution of iron sand in the Ulakan Tapakis region based on magnetic susceptibility values. Understanding how variations in magnetic susceptibility correlate with the mineralogical composition and concentration of iron-bearing minerals in the sediments is crucial for optimizing extraction processes and minimizing environmental impacts. This study hypothesizes that these variations influence the distribution of iron sand and aims to develop a model that accurately represents this relationship.

Research on iron sand has shown the significance of magnetic susceptibility in identifying areas rich in iron content. For instance, [2] demonstrated that iron sand deposits in Papua exhibit high mass-specific magnetic susceptibility, indicating areas with high iron concentrations. Additionally, [3] applied geoelectric resistivity methods for iron sand exploration in Ulakan Tapakis, underscoring the effectiveness of combining multiple geophysical techniques for detailed exploration. In the Ulakan Tapakis region, mineralogical analyses reveal that heavy minerals such as magnetite, titanomagnetite, and hematite contribute to elevated magnetic susceptibility values, which could serve as a guide for mapping iron sand distribution more effectively [4,5].

This study aims to create a detailed model of iron sand distribution based on magnetic susceptibility in Ulakan Tapakis. Through field sampling, laboratory analysis, and microscopy, we will analyze iron sand's mineralogical composition and susceptibility to identify regions with high mineral potential. These findings are expected to support sustainable resource management and offer insights for future mineral exploration in similar coastal regions.

2. MATERIALS AND METHODS

2.1 Sampling and Laboratory Analysis

The sampling design involved using the hand bore method. Sampling was conducted at 20 drill points divided into four parallel transects along the coastline and five perpendicular transects to the coastline (Figure 1). The distance between parallel drill points was approximately 60 meters, totalling around 180 meters. The perpendicular drill points had a spacing of approximately 15 meters, totalling about 60 meters. The sampling process using the handbor method involved several steps: selecting the drill points, setting up the drilling equipment, connecting the drill bit and rods securely, and lifting the drill when the bit was filled. The drilling depth and soil description were recorded at each level, noting soil type, color, and condition. This process was repeated at 20 drill points with depths of 0-1.5 meters each. This scheme is in accordance with the technical guidelines for iron sand exploration issued by the

Mineral Resource Inventory Directorate Team [6]. Iron sand samples were collected from each drill hole for sample preparation, and the drill holes were refilled after sampling.

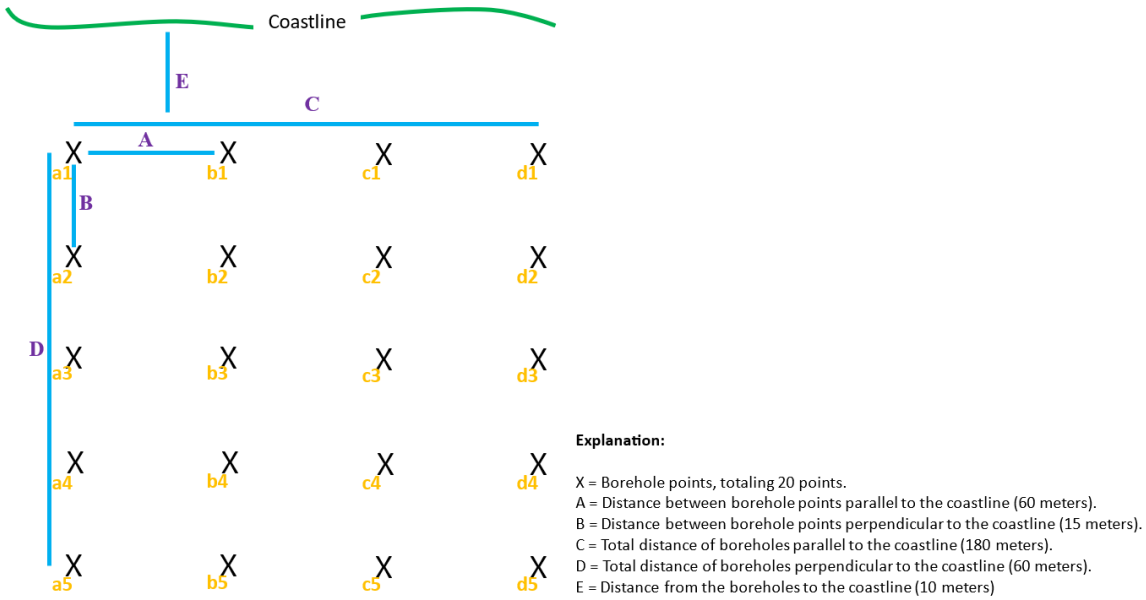

Figure 1: Distribution of iron sand sampling

The sample preparation followed the Japan Industrial Standard (J.I.S.) method. The drill samples were mixed in a container until homogenized and then divided into grid lines in an increment box. The samples were reduced using an increment spoon and stored in sample bags. These samples were then dried in an oven and divided into individual samples, composite samples, and duplicates.

The percentage of magnetic minerals (MM) in the iron sand was calculated by separating the magnetic minerals from the non-magnetic ones using a permanent magnet and weighing the resulting fractions. The MM percentage was computed using Equation (1):

$$MM(\%) = \frac{magnetic\ mineral\ mass}{total\ mass\ of\ sand} \times 100\% \quad (1)$$

The Magnetic Susceptibility Testing process involved several steps, including weighing an empty sample holder, filling the holder with a prepared sample, labelling it, and performing calibration and multiple measurements (three times each for low-field and high-field susceptibility) to ensure accuracy. The Bartington Magnetic Susceptibility Meter (MS2B) was used to measure susceptibility. The measurement process included placing the sample in the instrument, recording susceptibility values, and comparing the results before and after putting the sample.

The collected data were processed to determine the magnetic mineral percentage and magnetic susceptibility values. These values were then used to create maps showing the distribution of magnetic minerals. Further analysis will be conducted using a microscope based on the highest magnetic mineral percentage and susceptibility values for all samples. This comprehensive methodology ensured a systematic and thorough investigation of the iron sands' magnetic susceptibility and mineral content in the Ulakan Tapakis area, providing valuable insights into their potential and quality.

2.2 Microscopy and Elemental Identification

Standard optical microscopy techniques were employed to characterize the grain morphology and mineral composition of sample with the highest magnetic response. Grains from the sample were mounted on glass slides and examined using a Meiji Techno MT9930 polarizing microscope in both

transmitted-light and reflected-light modes. This instrument provided high-resolution imaging suitable for detailed mineralogical observation. Transmitted plane-polarized light enabled the identification of translucent minerals, while reflected light facilitated the examination of opaque, metallic grains. Individual mineral grains were visually identified based on their optical properties, including inherent color, crystal habit (grain shape), relief, and surface luster or reflectivity. Iron-bearing minerals were distinguished by their dark, metallic, opaque appearance. In contrast, zirconium-associated minerals were recognized by their high-relief, prismatic, and translucent morphology, consistent with known characteristics of zircon. These visual criteria offered a qualitative framework for identifying key mineral species: iron oxide minerals (likely magnetite or ilmenite) appeared as black, light-blocking grains with reflective surfaces in reflected light, whereas potential zircon grains appeared colorless to pale with distinct relief and well-formed crystal outlines under transmitted light.

3. RESULTS AND DISCUSSION

3.1 Cross-section Modeling

The study involves twenty borehole points, strategically positioned with a 60-meter interval parallel to the coastline and a 15-meter interval perpendicular to it. The distance of each borehole from the coastline is set at 10 meters, with borehole depths ranging from 0 to 1.5 meters. Each borehole points reveal varying lithological compositions, displaying medium sand (0.25-0.55 mm), fine sand (0.125-0.25 mm), and silt (0.004-0.625 mm). The lithological profiles of the lines, as depicted in Figure 2 highlight distinct stratifications of these materials across different sections of each line.

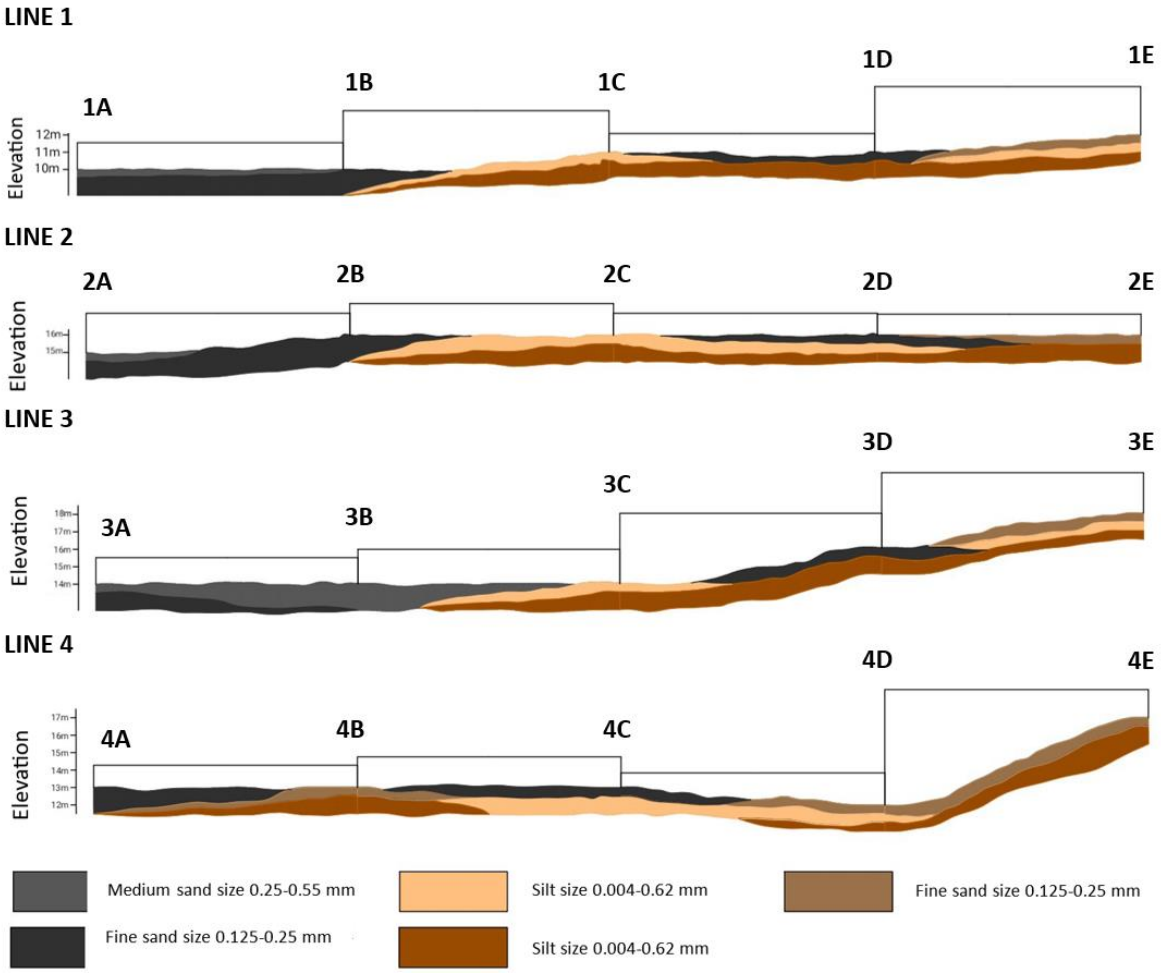

Figure 2: Cross-section of iron sand sampling transect

The material distribution across the different points reveals a varied and intricate sedimentary environment, characterized by a range of textures, colors, and moisture levels. For Line 1, the segment between points 1A and 1B features medium grey sand (0.25-0.55 mm) and dark grey fine sand (0.125-0.25 mm). Between 1B and 1C, the composition includes dark grey fine sand (0.125-0.25 mm), dry light brown silt (0.004-0.625 mm), and moist dark brown silt (0.004-0.625 mm). Moving from 1C to 1D, there is a continuation of dry light brown silt, moist dark brown silt, and dark grey fine sand. Finally, between 1D and 1E, the materials transition to dark grey fine sand, greyish brown fine sand, and moist dark brown silt, indicating a mix of sedimentary deposits in this line.

Line 2 continues this complex pattern. The materials between points 2A and 2B consist of medium grey sand and dark grey fine sand. From 2B to 2C, there is a notable presence of medium sand that is dark grey and moist, along with dry light brown silt and moist dark brown silt. Between 2C and 2D, the materials shift to dry light brown silt, moist dark brown silt, and dark grey fine sand. Lastly, from 2D to 2E, there are deposits of dark grey fine sand, dry light brown silt, moist dark brown silt, and dry greyish brown silt. This diverse composition highlights the variability in sediment deposition along Line 2.

In Line 3, the segment between points 3A and 3B reveals medium grey sand (0.25-0.55 mm) and blackish grey iron sand (0.0625-0.125 mm) with a moist texture. The materials between points 3B and 3C include medium grey sand, light brown silt (0.004-0.625 mm), and dark brown silt. From 3C to 3D, there is light brown silt, dark brown silt, and dark grey medium sand. Finally, between points 3D and 3E, the materials consist of dark grey medium sand, greyish brown fine sand (0.125-0.25 mm), and dark brown silt. This line illustrates a blend of medium and fine sands with varying silt compositions, reflecting the dynamic sedimentary processes in the area.

Line 4 presents a mix of medium and fine sands and various silt deposits. The materials between points 4A and 4B are medium dark grey sand, greyish brown medium sand, and moist dark brown medium sand. From 4B to 4C, there are deposits of greyish brown medium sand, moist dark brown medium sand, dark grey medium sand, and moist light brown silt. Between 4C and 4D, the composition includes dark grey medium sand, brownish-grey fine sand, and dark brown silt. Lastly, from 4D to 4E, the materials transition to dark grey fine sand and dark brown silt. This line showcases diverse sediment types, further illustrating the complex depositional environment.

The lithological analysis confirms the presence of iron sand, rich in magnetic minerals like magnetite, hematite, and maghemite, aligning with [7] on the material's utility in producing microwave absorbers. The natural formation processes of iron sand, involving the confluence of rivers and seas, lead to the sedimentation of these magnetic minerals, consistent with the observations of [8]. The compositional analysis of the iron sand samples is comparable to previous studies by [9], which identified magnetite as the predominant component, along with significant amounts of hematite and maghemite.

3.2 Percentage of Magnetic Minerals

To calculate the percentage of magnetic minerals in a sample, one must first determine the magnetic susceptibility of the minerals present. Magnetic susceptibility is a measure of how easily a material can be magnetized in the presence of an external magnetic field. One can estimate the percentage of magnetic minerals in the sample by measuring the magnetic susceptibility of a sample and comparing it to a standard reference material.

The analysis of the borehole samples, as presented in Table 1, reveals significant variations in the magnetic mineral content across different sampling points. The highest magnetic mineral content is observed at point 1D, with a value of 28.63%, while the lowest is at point 3C, with a value of 4.12%. The range of magnetic mineral content across all 20 borehole points spans from 4.12% to 28.63%. This variation indicates the heterogeneous distribution of magnetic minerals within the study area.

Table 1: Percentage of Magnetic Mineral Content (MM)

No	Point	Easting	Northing	Total Mass (gr)	Magnetic Mineral Mass (gr)	MM (%)
1	1A	631151.2	9923220.2	250.77	60.44	24.10%
2	1B	631159.2	9923225.1	250.24	38.34	15.32%
3	1C	631164.8	9923240.2	250.1	13.34	5.33%
4	1D	631171.3	9923255.8	250.28	71.66	28.63%
5	1E	631186.1	9923266.2	250.12	18.25	7.30%
6	2A	631112.3	9923257.4	250.46	31.04	12.39%
7	2B	631121.2	9923265.3	250.53	23.24	9.28%
8	2C	631132.4	9923278.2	250.43	15.51	6.19%
9	2D	631137	9923291.1	250.41	58.3	23.28%
10	2E	631150.3	9923298.8	250.4	35.77	14.29%
11	3A	631079.2	9923292.7	250.3	57.51	22.98%
12	3B	631101.8	9923301	250.47	18.19	7.26%
13	3C	631103.6	9923309.9	250.24	10.31	4.12%
14	3D	631110.1	9923316.9	250.89	26.61	10.61%
15	3E	631121.2	9923327.7	253.07	43.48	17.18%
16	4A	631045.5	9923328	250.67	38.17	15.23%
17	4B	631052.3	9923329.5	250.2	46.87	18.73%
18	4C	631061.6	9923342.1	250.17	15.61	6.24%
19	4D	631071.2	9923352.3	250.13	24.03	9.61%
20	4E	631082.3	9923365.5	250.89	26.54	10.58%

The observed range of magnetic mineral content aligns with previous findings in the literature. For instance, [10] highlights the importance of magnetic susceptibility in determining the induced magnetism of rocks containing magnetic minerals. The variations in magnetic mineral content can be influenced by factors such as the magnetizing field strength and the inherent properties of the minerals, as noted by [11]. This alignment of varying magnetic mineral concentrations across different borehole points suggests potential implications for resource exploration.

Understanding the distribution of magnetic minerals is crucial for various applications, from geological exploration to mineral processing. The high magnetic mineral content at specific points, such as 1D, indicates potential zones for targeted exploration and extraction of valuable resources, as suggested by [12]. Additionally, the micromagnetic models employed in the study provide insights into the internal magnetic configurations of minerals, aiding in more accurate predictions and analyses [13]. The importance of integrating geophysical and mineralogical data to optimize resource utilization and advance our understanding of magnetic properties in geological contexts.

Figure 3 presents a contour map depicting the spatial distribution of magnetic mineral content across the study area. The map uses a color gradient from blue (low content) to red (high content), with percentages indicated in the legend. Contour lines represent changes in magnetic mineral content, with

closer lines indicating steeper gradients. High magnetic mineral content is concentrated near point 1D, which ranges from 28% to 29%, while lower content is found around point 3C, ranging from 4% to 6%. The map reveals a varied distribution of magnetic minerals, with distinct high-content zones surrounded by lower-content areas.

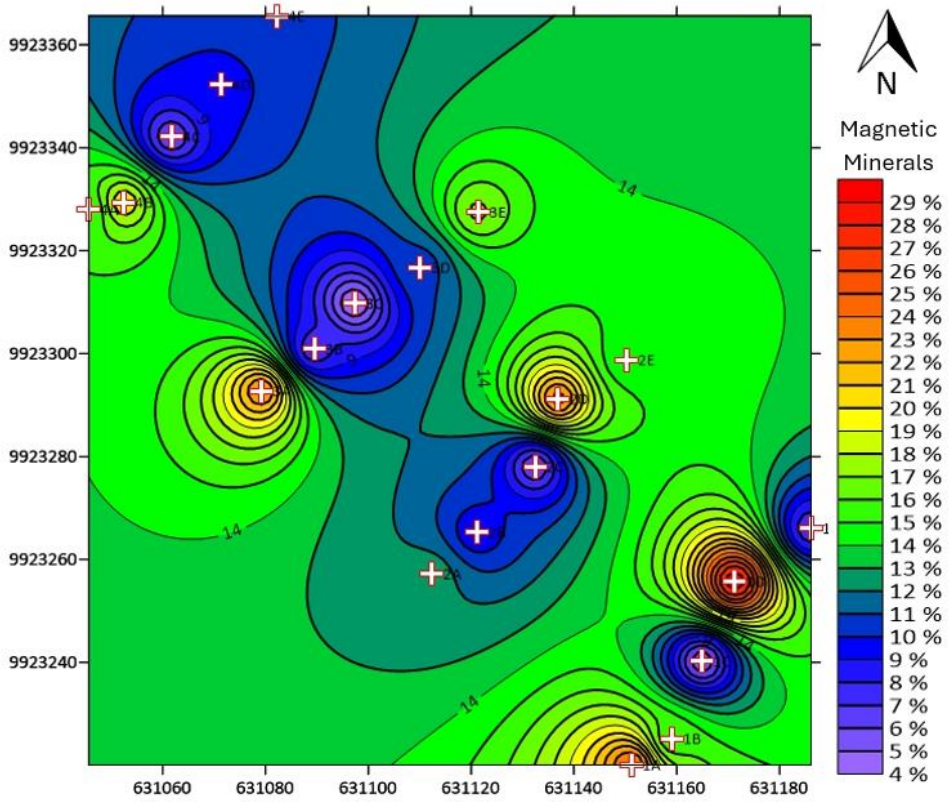

Figure 3: Magnetic mineral map

3.3 Magnetic Susceptibility

The measurement of magnetic susceptibility values was conducted using the Bartington instrument with the MS2B sensor under conditions of low field susceptibility (χlf) and high field susceptibility (χhf), with each measurement repeated three times. The MS2B sensor is used to measure magnetic susceptibility values based on the mass of the sample. Low field susceptibility measures a material's response to an applied magnetic field when the field strength is relatively low. It quantifies the degree to which a material can be magnetized under these conditions. Meanwhile, high field susceptibility is measured to understand how a material responds to a strong applied magnetic field. The magnetic susceptibility value in Ulakan Tapakis in every line is shown in Table 2.

The magnetic susceptibility measurements for each sample point, as detailed in Table 2, exhibit a significant range of values from 782.4 x 10-8 m³/kg to 5574.8 x 10-8 m³/kg. The highest magnetic susceptibility is observed at sample point 1D with a value of 5574.8 x 10-8 m³/kg, while the lowest value is recorded at sample point 4C with 782.4 x 10-8 m³/kg. The distribution of magnetic susceptibility across different lines shows varied ranges: Line 1 ranges from 991.2 x 10-8 m³/kg to 5574.8 x 10-8 m³/kg, Line 2 from 1050.0 x 10-8 m³/kg to 3644.5 x 10-8 m³/kg, Line 3 from 2182.4 x 10-8 m³/kg to 3987.9 x 10-8 m³/kg, and Line 4 from 782.4 x 10-8 m³/kg to 4798.3 x 10-8 m³/kg.

Table 2: Magnetic susceptibility in every sample point

No	Point	Easting	Northing	Low Field (χlf) (x10^{-8} m^3/Kg)	High Field (χhf) (x10^{-8} m^3/Kg)
1	1A	631151.19	9923220.18	3890.2	3858.5
2	1B	631159.23	9923225.1	3510.2	3481.5
3	1C	631164.8	9923240.15	991.2	984.1
4	1D	631171.3	9923255.8	5574.8	5536.5
5	1E	631186.14	9923266.24	3229.7	3208.6
6	2A	631112.25	9923257.35	3644.5	3610.4
7	2B	631121.22	9923265.34	2005.5	1989.3
8	2C	631132.35	9923278.23	1050	1040.7
9	2D	631136.99	9923291.13	1986.1	1969.8
10	2E	631150.29	9923298.8	2822.8	2802.6
11	3A	631079.18	9923292.68	3987.9	3969
12	3B	631101.76	9923300.97	2182.4	2179.8
13	3C	631103.6	9923309.87	2645	2626.6
14	3D	631110.11	9923316.93	2406.5	2388.1
15	3E	631121.24	9923327.67	3605.6	3580.3
16	4A	631045.49	9923328	1482.2	1470.8
17	4B	631052.29	9923329.53	4798.3	4754.5
18	4C	631061.57	9923342.12	782.4	776.9
19	4D	631071.16	9923352.26	1626.9	1613.8
20	4E	631082.3	9923365.46	3125.4	3103

The range of magnetic susceptibility values observed in this study aligns with the general understanding of magnetic susceptibility as a critical property that describes the magnetizability of materials when subjected to an external magnetic field [14]. The high susceptibility values, particularly at sample point 1D, suggest a significant concentration of magnetic minerals, consistent with [10] regarding the positive magnetic susceptibility of rocks containing magnetic minerals. Moreover, the variability in susceptibility values can be attributed to the differences in mineral compositions and depositional conditions, as noted by [15] in their study of sedimentary deposits.

The higher magnetic susceptibility values observed in Line 1 compared to the other lines suggest that this area might have a higher concentration of iron sand, which could be due to the depositional environment, possibly a basin or other geological feature that favors the accumulation of magnetic minerals. This aligns with [16], who discussed the significance of magnetic susceptibility in understanding sedimentary processes. Additionally, the general range of magnetic susceptibility values in the Ulakan Tapakis coastal area, from 782.4 x 10-8 m³/kg to 5574.8 x 10-8 m³/kg, indicates a substantial presence of magnetic minerals, which has implications for mineral exploration and processing. It can inform further studies and industrial applications, particularly in the optimization of magnetic separation techniques, as highlighted by [17] in their analysis of magnetic properties.

3.4 Microscopy Analysis

Microscopy analysis was conducted on the iron sand sample from point 1D, which was selected due to its high magnetic susceptibility (5574.8 × 10^{-8} m³/kg) and magnetic mineral content (28.63%). Through this method, the dominant presence of iron (Fe) was inferred from black to dark grey, opaque, metallic grains, while zirconium-bearing minerals (Zr) were indicated by translucent, prismatic grains with high relief, consistent with zircon morphology.

The observed average grain size was approximately 0.21 mm for Fe-rich grains and 0.32 mm for other non-ferromagnetic minerals. The visual estimation, although qualitative, suggested a sample composition of approximately 79.98% Fe and 20.02% other minerals, in alignment with the gravimetric and susceptibility data obtained from prior analyses.

These results, illustrated in Figure 4, demonstrate the heterogeneity and mineralogical complexity of the sample. The high Fe content and relatively fine grain size make this material potentially valuable for magnetic-based industrial applications, such as metallurgical processes and microwave absorber materials [18,19]. Although Zr is less abundant, its presence may offer additional value in specialized industrial contexts [20]. The application of SEM-EDS and XRF techniques proves essential for detailed characterization, supporting their broader use in iron sand mineral exploration [21-23].

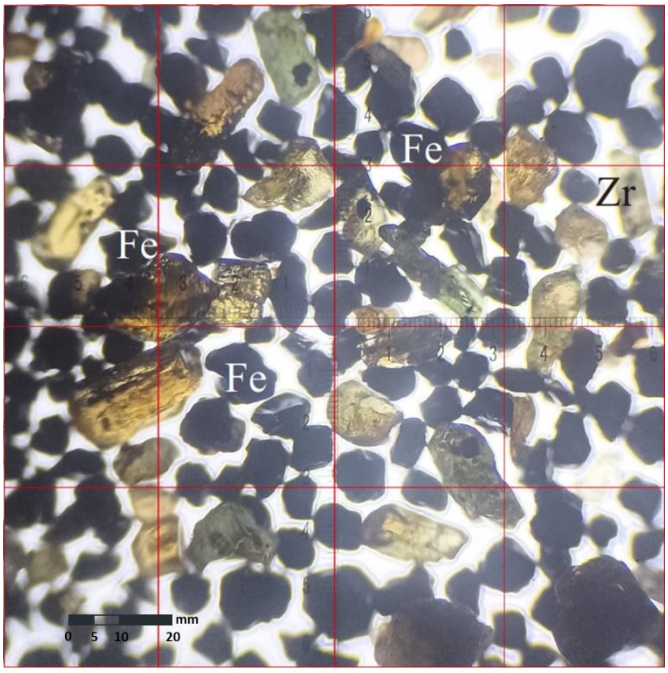

Figure 4: Optical micrograph of a sample at point 1D

4. CONCLUSIONS

This study provides a detailed analysis of the mineralogical and magnetic properties of iron sand deposits in the Ulakan Tapakis coastal area. The highest magnetic mineral content was identified at point 1D, with a concentration of 28.63% and magnetic susceptibility values reaching 5574.8 x 10^{-8} m^3/kg in the low field and 5536.5 x 10^{-8} m^3/kg in the high field. Microscopy analysis confirmed that iron (Fe) is the predominant mineral, making up 79.98% of the sample. These findings underscore the heterogeneous distribution of iron sand and highlight high-potential zones for exploration. The novel application of magnetic susceptibility measurements combined with mineralogical composition mapping offers valuable insights for targeted extraction, with implications for resource management and industrial applications. Future research could enhance these findings by refining analysis techniques and exploring broader uses of iron sand.

Acknowledgements

We would like to express our sincere gratitude to the Department of Mining Engineering, particularly the Exploration Laboratory, for providing the facilities and technical guidance essential to

the field and laboratory analyses. We also extend our appreciation to Biro Sequence'22 for their valuable assistance in the sample processing phase. Furthermore, we are thankful to the local authorities and officials of Nagari Ulakan Tapakis for granting access and supporting our fieldwork activities throughout the study.

Author Contributions

All authors contributed toward data analysis, drafting and critically revising the paper and agree to be accountable for all aspects of the work.

Disclosure of Conflict of Interest

The authors have no disclosures to declare

Compliance with Ethical Standards

The work is compliant with ethical standards

References

[1] Octova, A., Anaperta, Y. M., Febriandika, H. G., Martinus, H., Nazki, A., Razi, P. & Putra, A. (2022). 3D modelling of iron sand using geoelectrical resistivity method with wenner array in Ulakan Tapakis, Padang Pariaman, West Sumatra. In Journal of Physics: Conference Series, The 4th International Conference on Research and Learning of Physics (ICRLP 2021), Padang, Indonesia, 31 August–2 September 2021.

[2] Togibasa, O., Bijaksana, S. & Novala, G. C. (2018). Magnetic properties of iron sand from the Tor River Estuary, Sarmi, Papua. *Geosciences,* 8(4), 113.

[3] Octova, A., Anaperta, Y. M., Febriandika, H. G., Martinus, H., Nazki, A., Razi, P. & Putra, A. (2022). Application of geoelectrical resisivity method for iron sand exploration in Ulakan Tapakis Padang Pariaman. In Journal of Physics: Conference Series, The 4th International Conference on Research and Learning of Physics (ICRLP 2021), Padang, Indonesia, 31 August–2 September 2021.

[4] Harahap, L. M. L., Idrus, A., Sukadana, I. G. & Handayani, T. (2023). Mineralogical distribution and characteristics of fe-, ti-, and v-bearing beach ironsand deposit in Adikarto Bay Kulonprogo, Yogyakarta, Indonesia. In IOP Conference Series: Earth and Environmental Science, The 3rd Geoscience and Environmental Management symposium, online, 7–8 September 2022.

[5] Rahmi, A., Rifai, H., Rahmayuni, R., Yuwanda, A. N., Visgun, D. A. & Dwiridal, L. (2022). Irregular magnetic susceptibility pattern of iron sand from pasia jambak beach, Pasia Nan Tigo, Padang, Indonesia. In Journal of Physics: Conference Series, The 4th International Conference on Research and Learning of Physics (ICRLP 2021), Padang, Indonesia, 31 August–2 September 2021.

[6] Tim Direktorat Inventarisasi Sumberdaya Mineral (2005). *Pedoman Teknis Eksplorasi Pasir Besi.* (Pusat Sumberdaya Geologi) pp. 1-17.

[7] Susilawati, S., Doyan, A. & Hadisaputra, S. (2022). Analysis magnetic mineral content of natural iron sand in beach island Lombok as basic materials of micro wave absorbers. *Jurnal Penelitian Pendidikan IPA*, 8(4), 1755-1758.

[8] Visgun, D. A., Rifai, H., Rahmayuni, R., Yuwanda, A. N., Rahmi, A. & Dwiridal, L. (2022). Identification of rock types from iron sand at Pasia Jambak Beach, Padang, West Sumatra. In Journal of Physics: Conference Series, The 4th International Conference on Research and Learning of Physics (ICRLP 2021), Padang, Indonesia, 31 August–2 September 2021.

[9] Haryati, E., Dahlan, K., Bunga, M., Napitupulu, D. & Togibasa, O. (2021). Mineral content and magnetic properties of river iron sand from Jayapura, Papua. *Journal of Magnetism and Its Applications*, 1(2), 30-33.

[10] Khawaja, A. M., Ahmed, O. Q., Alkhalidy, A. A., Manii, J. K., Almamori, H. O. & Salman, K. J. (2024). Using gradiometric technique to prospect archaeological features in Tell Al-Deylam, South of Babylon City, Middle of Iraq. In IOP Conference Series: Earth and Environmental Science, 3rd Scientific Conference of Iraqi Desert Geology (IDGC 2023), Ramadi, Iraq, 13–15 December 2023.

[11] Oliveira, J. S., Wieczorek, M. A. & Kletetschka, G. (2017). Iron abundances in lunar impact basin melt sheets from orbital magnetic field data. *Journal of Geophysical Research: Planets*, 122(12), 2429-2444.

[12] Berndt, T. A. & Chang, L. (2018). Theory of stable multidomain thermoviscous remanence based on repeated domain wall jumps. *Journal of Geophysical Research: Solid Earth,* 123(12), 10-399.

[13] Cortés-Ortuño, D., Fabian, K. & de Groot, L. V. (2022). Mapping magnetic signals of individual magnetite grains to their internal magnetic configurations using micromagnetic models. *Journal of Geophysical Research: Solid Earth*, 127(5), e2022JB024234.

[14] Deistung, A., Schweser, F. & Reichenbach, J. R. (2017). Overview of quantitative susceptibility mapping. *NMR in Biomedicine*, 30(4), e3569.

[15] Pas, D., Da Silva, A. C., Poulain, G., Spassov, S. & Boulvain, F. (2019). Magnetic susceptibility record in Paleozoic succession (Rhenohercynian Massif, Northern Europe)–disentangling sea level, local and diagenetic impact on the magnetic records. *Frontiers in Earth Science*, 7, 341.

[16] Lai, C. H., Lu, M. Y. & Chen, L. J. (2012). Metal sulfide nanostructures: synthesis, properties and applications in energy conversion and storage. *Journal of Materials Chemistry*, 22(1), 19-30.

[17] Bergsland, N., Schweser, F., Dwyer, M. G., Weinstock‐Guttman, B., Benedict, R. H. & Zivadinov, R. (2018). Thalamic white matter in multiple sclerosis: A combined diffusion‐tensor imaging and quantitative susceptibility mapping study. *Human Brain Mapping*, 39(10), 4007-4017.

[18] Eslahpazir, R., Liu, Q. & Ivey, D. G. (2012). Characterization of iron-bearing particles in Athabasca oil sands. *Energy & Fuels*, 26(8), 5036-5047.

[19] Khwaja, H. A., Aburizaiza, O. S., Hershey, D. L., Siddique, A., Guerrieri, P. E. D. A., Zeb, J., Abbass, M., Blake, D. R., Hussain, M. M., Aburiziza, A. J., Kramer, M. A. & Simpson, I. J. (2015). Study of black sand particles from sand dunes in Badr, Saudi Arabia using electron microscopy. *Atmosphere*, 6(8), 1175-1194.

[20] Didik, L. A., Damayanti, I., Jumliati, J. & Lestari, P. A. (2021). Morphological characteristics and mineral content analysis of magnetic minerals based on river and coastal sand using SEM-EDX. J. *Sains Dasar*, 10(2), 44-50.

[21] Rianna, M., Sembiring, T., Situmorang, M., Kurniawan, C., Setiadi, E. A., Tetuko, A. P., Simbolon, S., Ginting, M. & Sebayang, P. (2018). Characterization of natural iron sand from Kata Beach, West Sumatra with high energy milling (Hem). *Jurnal Natural*, 18(2), 97-100.

[22] You, Q., Yang, Z., Ma, J., Yan, X., Sesay, T., Wang, H. & Liang, Z. (2022). Analysis of the particle characteristics of aeolian sand in Yulin Area, China. *Advances in Civil Engineering*, 2022(1), 1-12.

[23] Al-Awah, H. & Matter, W. S. (2023). Physicochemical characterization and origin of aeolian sand dunes in Southeastern Qatar: A comparative study with Mediterranean sand dunes. *Advances in Geosciences*, 63, 1-13.